THE AMERICAN SOCIETY OF MECHANICAL ENGINEERS
345 E. 47 St., New York, N.Y. 10017

84-WA/DSC-12

Nagurka, M.L., Wormley, D.N., and Hedrick, J.K., "Dynamic Curving Performance of Rail Transit Vehicles," ASME Technical Paper 84-WA/DSC-12, ASME Winter Annual Meeting, New Orleans, LA, 1984.

Printed in USA.

Dynamic Curving Performance of Rail Transit Vehicles

M. L. NAGURKA
Department of Mechanical Engineering
Carnegie-Mellon University
Pittsburgh, PA 15213

and

D. N. WORMLEY
J. K. HEDRICK
Department of Mechanical Engineering
Massachusetts Institute of Technology
Cambridge, MA 02139

ABSTRACT

This paper addresses the dynamic curving performance of rail transit vehicles operating with conventional, self-steered, and forced-steered trucks. The influence of uspension design and wheel/rail profile geometry on vehicle dynamic response during curve entry is studied using a computer simulation model. The model incorporates wheel/rail creep force saturation, nonlinear suspension elements, rail lateral flexibility, and nonlinear wheel/rail geometry accounting for the possibility of two-point contact at any wheel. Curving performance is computed in terms of dynamic wheel/rail interaction forces, vehicle suspension and body forces, vehicle displacements and velocities, and wear indices such as the work done by creep forces in the wheel/rail contact patches. The results show the presence of transient characteristics and essentially substantiate the results of steady-state analyses. The results suggest that vehicles with steered trucks, in particular forced-steered trucks, and single-point contact wheel profiles offer performance advantages compared to vehicles with conventional trucks and two-point contact profiles.

NOMENCLATURE

a	half of track gauge
b	half of wheelbase
$\underline{B}$	forcing function vector
c_o	secondary yaw viscous damping
c_{px}	primary longitudinal damping
c_{py}	primary lateral damping
c_{pz}	primary vertical damping
c_{sy}	secondary lateral damping
c_{sz}	secondary vertical damping
$\underline{C}$	damping matrix
d_p	half of lateral spacing between primary longitudinal springs
d_s	half of lateral spacing between secondary vertical springs
G	track curvature steering gain
h_{cs}	vertical distance from secondary suspension to carbody center of mass
h_{tp}	vertical distance from primary suspension to truck center of mass
h_{ts}	vertical distance from truck center of mass to secondary suspension
I_{cx}	roll principal mass moment of inertia of carbody
I_{cz}	yaw principal mass moment of inertia of carbody
I_{tx}	roll principal mass moment of inertia of truck frame
I_{tz}	yaw principal mass moment of inertia of truck frame
I_{wy}	pitch principal mass moment of inertia of wheelset
I_{wz}	yaw principal mass moment of inertia of wheelset
k_{b2}	interaxle bending stiffness
k_{px}	primary longitudinal suspension stiffness
k_{py}	primary lateral suspension stiffness
k_{pz}	primary vertical suspension stiffness
k_{sy}	secondary lateral suspension stiffness
k_{sz}	secondary vertical suspension stiffness
k_{s2}	interaxle shear stiffness
$\underline{K}$	stiffness matrix
ℓ_s	half of truck center pin spacing
$\underline{M}$	mass matrix
r_o	rolling radius for centered wheelset
W_c	carbody weight
W_T	truck frame weight

W_w	wheelset weight
$\underline{X}$	displacement state vector
y_{fc}	flange clearance
y_{rL}, y_{rR}	lateral displacement of left, right rail
y_w	lateral displacement of wheelset
Δy	cant deficiency steering offset
$\Delta\psi$	track curvature steering offset
ψ_c	carbody yaw angle with respect to local tangent
ψ_w	wheelset angle of attack, or yaw angle with respect to radial alignment

Conversion Factors

1 deg	=	0.01745 rad
1 ft = 12 in	=	0.3048 m
1 lb	=	4.448 N
1 mph	=	0.4470 m/sec
1 slug	=	14.59 kg

INTRODUCTION

The curve negotiation ability of rail transit vehicles significantly influences both operational performance and maintenance requirements. During curve negotiation the rate of wear at the wheels and rails is accelerated, the fuel consumption is increased, the potential danger of derailment is heightened, and objectionable screeching noise is often generated compared to tangent track operation. Rapid wheel and rail wear, a problem experienced by several urban transit systems, necessitates frequent wheel reprofiling and rail renewal and increases maintenance costs [1, 2].

Several proposals have been suggested to improve curving performance. These proposals include the use of vehicles with:

1. Conventional trucks employing suspension components between the axles and truck frame which have reduced stiffness [1, 3, 4].
2. Self-steered (radial) trucks, employing direct interconnections between the axles, which rely on wheel/rail creep forces to help align the wheelsets radially in curves [2, 5-8].
3. Forced-steered trucks, employing direct interconnections between the axles as well as (passive) linkage connections between the axles and carbody, which "force" the wheelsets into nominally radial positions in curves [9-12].
4. Wheel profiles which offer a smooth transition from tread to flange and which maintain single point wheel/rail contact in curves [13-16].

These proposals have been motivated primarily by the desire to reduce wheel and rail wear by achieving wheelset radial alignment during curve negotiation while maintaining adequate dynamic stability to avoid hunting during tangent track operation.

Steady-state studies [17, 18] have indicated the value of modifying suspension design and wheel/rail profile to minimize wheelset angles and wheel/rail forces and thus reduce wheel and track wear. In particular, the steady-state studies have shown that significant improvements in curving performance (in terms of decreased wheel/rail contact work) are possible without loss of dynamic stability by employing forced-steered trucks in comparison to conventional and self-steered trucks. Further, the steady-state studies have demonstrated the advantage in terms of reduced contact work during curve negotiation of using single-point contact wheel/rail profiles compared to two-point contact profiles.

Steady-state conditions are rarely encountered. Most often dynamic effects occur due to deliberate and unintentional changes in track curvature, gauge, and banking. Deliberate changes are imposed in sections of spiral transition track, such as curve entry and exit sections; unintentional changes occur due to track irregularities.

Literature Review

In the last decade, nonlinear dynamic curving analyses have been conducted relying heavily on large-scale computer systems. Smith [19], Law and Cooperrider [20, 21], Clark [22], Duffek and Jaschinski [23], and Fortin and Anderson [24] have developed detailed nonlinear computer models that predict vehicle transient response during curve negotiation. Their models assume that each wheel of a vehicle contacts the rails at a single point. Single-point contact is an acceptable approximation of tread contact. For some profiles, such as the new AAR[1] wheel profile, single-point contact is not an appropriate model of flange contact since two-point tread and flange contact occurs [13, 14]. Previous steady-state studies [15, 16] have shown that significant errors result in predicting curving behavior based on analyses assuming single-point wheel/rail contact when two-point contact occurs. In this work the effect of two-point contact is included in a dynamic curving study.

Scope of Paper

This study addresses the dynamic curving behavior of rail vehicles caused by deliberate changes in track curvature and banking. A dynamic curving computer simulation model is developed that predicts vehicle displacements and velocities as well as wheel/rail transient forces and contact work. The model is used to study the curve entry performance of vehicles with conventional, self-steered, and forced-steered trucks running with new AAR and Heumann wheels.

STUDY METHODOLOGY

During curve negotiation, different performance objectives can be identified, including perfect steering, prevention of derailment, minimum wheel/rail forces, and minimum wheel/rail wear. Accordingly, various performance indices have been proposed to represent the ability of a rail vehicle to negotiate a curve [16]. Examples of curving performance indices used in this paper are wheelset lateral excursions, wheelset angles of attack, wheel/rail lateral forces, and wheel/rail contact work (a wheel/rail wear index defined as the dot product of the resultant creep force and creepage vectors).

Track Model

A simple model of smooth track is adopted in which sections of tangent track and constant radius curve track are coupled by sections of quadratically faired transition track. In the sections of transition track, the track curvature and superelevation angle are approximated by second-order polynomial functions. Such quadratically faired transition spiral track has been used in [20, 21].

Each rail of the track is assumed to have lateral flexibility. Rail rollover or overturning motion is neglected. Each rail is modeled in the lateral direction as possessing effective viscous damping and linear stiffness with negligible effective inertia. Typical values of effective lateral stiffness are 1.0×10^5 lb/ft for soft rail and 1.0 x

[1] Association of American Railroads.

10^7 lb/ft for stiff rail [25]. A representative value of effective lateral damping is 1.0×10^4 lb-sec/ft.

Wheelset Model

The wheelset represents the basic element of the rail vehicle steering and support system. An analytical model has been developed to characterize the dynamic behavior of a wheelset negotiating smooth, laterally flexible, curved track [26]. The model represents single-point and two-point wheel/rail contact at the flanging wheel and accounts for nonlinearities due to wheel/rail profile geometry and due to cubic saturation of the resultant creep force to the adhesion limit. The governing wheelset and rail equations of motion represent force and moment dynamic equilibrium equations.

Assuming continuous wheel/rail contact and curve negotiation at constant forward speed, the governing equations of motion represent a system of five states for the wheelset and two states for the rails. The five states of the wheelset are the lateral displacement and velocity, the yaw angle and rate, and the spin speed. In general, the spin speed will differ from the pure rolling angular speed due to creepage at the wheels. Each rail has a state to describe its lateral motion. When two-point contact occurs, the state of the rail at the flanging wheel is known due to a geometric constraint relation that exists between the wheelset and rail lateral motions. For example, for two-point contact at the left wheel,

$$y_W - y_{rL} = y_{fc} \tag{1}$$

where y_W and y_{rL} are the lateral displacements of the wheelset and left rail, respectively, and y_{fc} is the flange clearance.

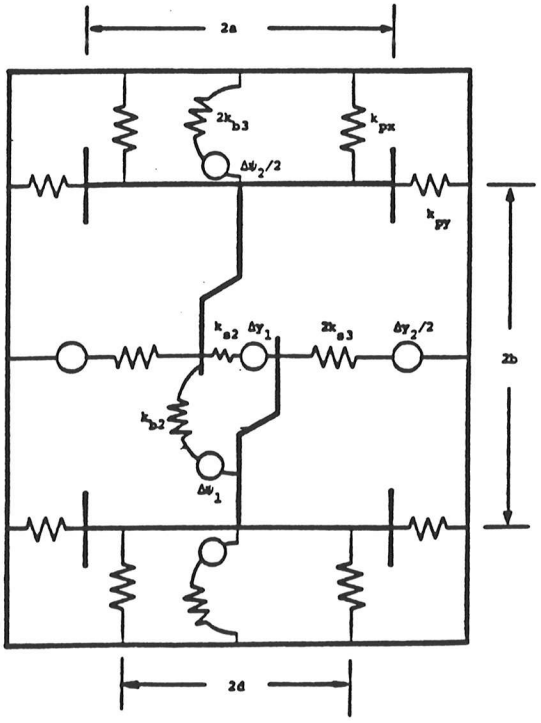

Figure 1. Generic Truck Model.

The contact geometry (rolling radius, contact angle) at each wheel is a function of the net lateral excursion and is specified by a wheel/rail profile geometry data table. The data table applies for a fixed rail gauge. Due to rail flexibility, the gauge changes and use of the fixed-gauge wheel/rail profile data represents an approximation. In this work, it is assumed that (1) the flanging wheel contact geometry is correct, and (2) the nonflanging wheel contact geometry is in error, but the error is small since the tread contact geometry is relatively constant.

Generic Truck Model

Two wheelsets are coupled to the generic truck model shown in Figure 1 by primary suspension elements. The primary suspension arrangement is modeled as a system of piecewise linear, hardening springs connected in parallel in the longitudinal and lateral directions with stiffnesses k_{px} and k_{py}, respectively. In addition, the generic truck model includes the effects of steering linkages between the wheelsets to represent self-steered trucks and steering linkages between the wheelsets, truck, and carbody to represent a variety of forced-steered truck designs. The effects of these forced-steered linkages are represented by geometric yaw offsets, $\Delta\psi_1$ and $\Delta\psi_2$, in series with linkage bending stiffnesses, k_{b2} and k_{b3}, and lateral offsets, Δy_1 and Δy_2 in series with linkage shear stiffnesses, k_{s2} and k_{s3}. The geometric yaw and lateral offsets are controlled by steering laws which are a function of the wheelset, truck, and carbody geometries [11, 17, 26].

The steering law for the forced-steered truck studied in this paper is given by

$$\left.\begin{aligned} \Delta\psi_1 = \pm\, 2G \left(\frac{y_{W1} - y_{W2}}{2b} - \psi_c\right) \\ + 2\left(\frac{G + 1}{b}\right)\left(\frac{y_{W1} + y_{W2}}{2} - y_T\right) \end{aligned}\right\} \tag{2}$$

and

$$\Delta\psi_2 = \Delta y_1 = \Delta y_2 = k_{b3} = k_{s3} = 0 \tag{3}$$

where y_{W1}, y_{W2}, and y_T are the lateral displacements of the leading wheelset, trailing wheelset, and truck, respectively; ψ_c is the yaw angle of the carbody; 2b is the truck wheelbase; and G is the steering gain. In eq. (2), the notation $\pm$ implies + for the front truck and - for the rear truck. The steering gain, G, is set equal to the gain which kinematically aligns the wheelsets radially, given by b/ℓ_s [26].

Vehicle Model

Two trucks are connected to a carbody to form the rail vehicle model. Each truck is coupled to the carbody by secondary suspension elements. The model of the secondary suspension system consists of linear springs connected in parallel in the lateral and vertical directions, and a coulomb damper in the yaw direction which saturates at the centerplate breakaway torque. For numerical convenience, the damper includes a linear viscous band at the origin which implies that the secondary yaw torques vanish in steady-state. The assumption of negligible steady-state secondary yaw torques does not represent a serious limitation since (1) this study focuses on vehicle transient behavior during curve entry, and (2) due to actual dynamic effects, the secondary torque probably does not remain at a constant breakaway level in steady-state, as predicted by a true coulomb damper [26].

Numerical Methods

A dynamic curving analysis has been developed to predict the dynamic behavior of the rail vehicle model as it enters and negotiates curved track. The behavior is described by coupled, nonlinear, differential equations of motion, which are derived in detail in [26].

The full vehicle model is characterized by 42 states: 20 states for the 4 wheelsets, 8 states for the 2 trucks, 6 states for the carbody, and 8 states for the rails. As noted, each wheelset has two degrees of freedom (i.e., 4 states) to describe its lateral and yaw motions, as well as a state to describe its spin speed. Each truck has two degrees of freedom to describe its lateral and yaw motions. The carbody is characterized by lateral, yaw and roll degrees of freedom. In addition, the rail at each wheel has a state to describe its lateral motion.

In matrix notation, the dynamic curving equations of motion of the full vehicle model can be written as:

$$\underline{M}\,\ddot{\underline{X}} + \underline{C}\,(\underline{X}, \dot{\underline{X}})\,\dot{\underline{X}} + \underline{K}\,(\underline{X}, \dot{\underline{X}})\,\underline{X} = \underline{B}\,(\underline{X}, \dot{\underline{X}}) \qquad (4)$$

where $\underline{M}$, $\underline{C}$, and $\underline{K}$ are mass, damping and stiffness matrices, respectively, $\underline{B}$ is a forcing function vector due to track curvature and cant deficiency (lateral unbalance), and $\underline{X}$ is a displacement state vector. The damping and stiffness matrices are functions of displacements and velocities due to nonlinear suspension components. Eq. (4) represents a set of coupled nonlinear differential equations which are solved by digital integration using a variable time-step fourth-order Runge-Kutta scheme. Once integrated, the dynamic curving computer model provides the time histories of the state variables, the wheel/rail contact forces, and the wheel/rail contact work.

For a vehicle running with two-point contact wheel/rail profiles, two-point contact can develop at the outer or inner wheels of any of the wheelsets, especially during violent curve entry. For each wheelset of the vehicle, three distinct possibilities of wheel/rail contact exist: (1) single-point contact can occur at both wheels; (2) two-point contact can occur at the outer wheel and single-point contact can occur at the inner wheel; or (3) two-point contact can occur at the inner wheel and single-point contact can occur at the outer wheel. Thus, for a vehicle with four wheelsets, 81 contact combinations are possible. A separate set of vehicle equations of motion can be written for each contact combination.

The dynamic curving computer model automatically accounts for the possiblity of two-point contact at any wheel or wheels of the vehicle. The model solves the vehicle equations associated with single-point contact at all wheels and evaluates whether or not a correct solution has been obtained. If a two-point contact wheel/rail profile is being used and the net wheelset excursion at any wheel equals the flange clearance, the solution is not correct. Then, without incrementing the time-step, a different set of vehicle equations is solved and, again, checked for consistency. A consistent (i.e., correct) two-point contact solution is obtained if positive normal forces are predicted at the two contact points at each flanging wheel. If the solution is still not correct, the procedure is continued until the set of vehicle equations associated with the appropriate wheel/rail contact conditions is solved (as determined by obtaining a consistent solution). A flowchart of the dynamic curving computer program appears in Figure 2.

In general, the integration scheme used in the computer model requires a small time-step for numerical stability. For the performance studies of this paper, a time-step of 0.00075 sec is used when tread contact occurs at all wheels. The time-step is automatically reduced to 0.0005 sec when flange contact occurs at any wheel. The solution

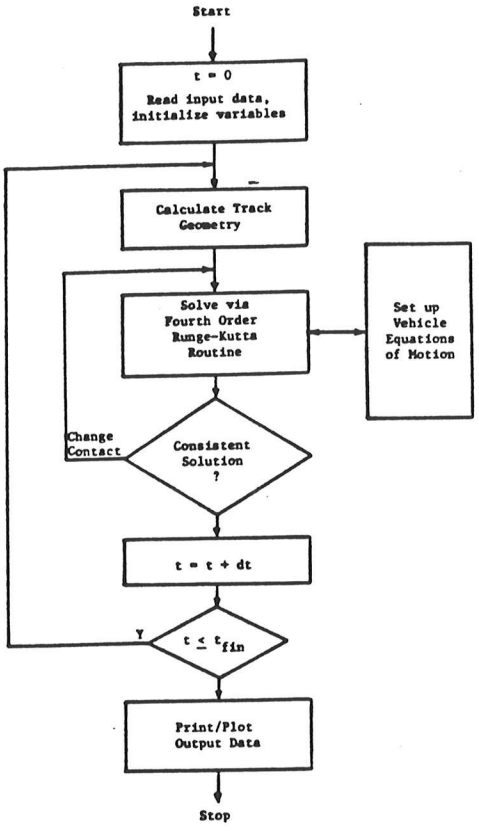

Figure 2. Flowchart of Dynamic Curving Program.

time required on a DEC VAX 11/780 computer is about 1 CPU minute for a 1 second simulation.

PERFORMANCE STUDIES

Curve entry performance studies have been conducted using the dynamic curving computer model with baseline rail and vehicle parameters. The parameters have been selected to represent typical conventional and advanced-design urban transit vehicles. Baseline vehicle parameters are listed in Table 1. The geometry, weights and inertias have been based on those reported for the existing and modified PATCO[2] Pioneer III trucks [2]. The baseline suspension stiffnesses have been chosen to yield vehicles with identical linear tangent track stability characteristics, i.e., critical speeds of 120 mph. For conventional trucks, the primary suspension values yielding the 120 mph critical speeds represent soft suspensions and provide improved curving performance compared to conventional trucks with standard primary suspensions [17].

Two wheel profiles have been identified to represent profiles characterized by single-point and two-point wheel/rail contact: a new AAR wheel and a Heumann wheel, respectively, both on worn rail of standard gauge. Both profiles have been obtained from tables in [27], smoothed, and modified to account for a centered rolling radius of 14.0 in. The new AAR wheel represents a wheel with a 1/20 tread taper and a steep flange at a flange clearance of 0.32

[2] Port Authority Transit Corporation.

Table 1. Baseline Vehicle Parameters.

GEOMETRY

r_o	[ft]	1.167	h_{ts}	[ft]	1.48
a	[ft]	2.32	h_{tp}	[ft]	0.52
b	[ft]	3.75	h_c	[ft]	2.375
d_p	[ft]	1.92	ℓ_s	[ft]	23.75
h_{cs}	[ft]	2.90	d_s	[ft]	3.71

COMPONENT WEIGHTS AND MOMENTS OF INERTIA

		Conventional Truck	Steered Trucks
W_w	[lb]	4054.	4854.
I_{wy}	[slug-ft^2]	28.	28.
I_{wz}	[slug-ft^2]	547.	946.
W_T	[lb]	4697.	4697.
I_{Tx}	[slug-ft^2]	1166.	1166.
I_{Tz}	[slug-ft^2]	1251.	1251.
W_c	[lb]	70,190.	
I_{cx}	[slug-ft^2]	4.40E4*	
I_{cz}	[slug-ft^2]	8.96E5	

BASELINE STIFFNESSES AND DAMPING

		New AAR Wheel	Heumann Wheel
Conventional			
k_{px}	[lb/ft]	1.35E5	6.50E5
c_{px}	[lb-sec/ft]	574.	2760.
Self-Steered			
k_{px}	[lb/ft]	1.20E5	5.00E5
c_{px}	[lb-sec/ft]	756	3150.
k_{b2}	[ft-lb/rad]	1.00E6	1.00E3
k_{s2}	[lb/ft]	1.00E6	1.00E6
Forced-Steered			
k_{px}	[lb/ft]	7.00E4	7.00E4
k_{b2}	[ft-lb/rad]	1.68E5	1.66E6
k_{s2}	[lb/ft]	1.00E6	1.00E6

All Vehicles:

k_{py}	[lb/ft]	7.50E5	k_{pz}	[lb/ft]	1.00E6
c_{py}	[lb-sec/ft]	620.	c_{pz}	[lb-sec/ft]	600.
k_{sy}	[lb/ft]	1.95E4	k_{sz}	[lb/ft]	2.04E4
c_{sy}	[lb-sec/ft]	1420.	c_{sz}	[lb-sec/ft]	1630.
c_o	[ft-lb-sec/rad]	1.00E7	T_o	[ft-lb]	7500.

in. The single-point contact Heumann wheel represents a wheel with a smooth transition from tread to flange and has an effective tread conicity of 0.20. Linear creep coefficients typical of the tread and flange of the two wheel profiles have been calculated using Hertzian contact theory.

In the curve entry simulations, the following assumptions are made: (1) The vehicles enter the transition spiral track at the initial time (t = 0.0 sec) from centered tangent track positions. (2) The vehicles operate at constant forward speed, determined by the balanced running speed for the constant radius curve track with 6 in superelevation. (3) The baseline transition spiral is 150 ft, which represents a typical length for transit systems. (4) Laterally stiff rails are used with a stiffness of 1.0×10^7 lb/ft. (5) The wheelsets are powered with axle-drive torques of 420 ft-lb, representing 5% of the slip torque for axles with 50 HP (27,500 ft-lb/sec) traction motors operating at 50 mph. (6) The wheel/rail coefficient of friction is 0.3.

Performance of Conventional Vehicles

The effect of track curvature, wheel/rail profile, and transition spiral length on the transient behavior of conventional vehicles is addressed in this section.

The nature of curve entry dynamics is shown in the response of a conventional vehicle with new AAR wheels negotiating a 150 ft transition spiral into a 10° (575 ft radius) curve at a balance speed of 45 ft/sec. Figures 3a and b show the wheelset lateral excursions and angles of attack, respectively, as functions of time. Figures 4a and b show the lateral force and contact work, respectively, at the leading outer (i.e., flanging) wheel as functions of time.

As the front truck enters the spiral curve, the leading wheelset rapidly displaces laterally toward the outer rail. The wheelset overshoots its desired rolling radius difference and thus the lateral displacement decreases slightly and then grows again. The leading outer wheel approaches its flange, but maintains single-point tread contact until it encounters the flange at t = 1.375 sec (i.e., 62 ft into the spiral). Two-point contact occurs at the leading outer wheel for the remainder of the simulation. The trailing wheelset of the front truck shows similar but somewhat lagged behavior. It displaces laterally maintaining single-point tread contact until the outer wheel impacts its flange at t = 3.000 sec (i.e., 135 ft into the spiral). It stays in two-point tread and flange contact for the remainder of the simulation.

The leading and trailing wheelsets of the rear truck displace rapidly toward the outer rail at t ≅ 2.0 sec (i.e., ≅ 90 ft into the spiral). The leading outer wheel of the rear truck impacts its flange at t = 2.250 sec (i.e., 101 ft into the spiral) causing two-point contact to occur momentarily and, then, bounces back into tread contact until t = 2.750 sec (i.e., 124 ft into the spiral). At all subsequent times two-point contact occurs at the leading outer wheel of the rear truck. The trailing wheelset of the rear truck maintains single-point tread contact during the entire transition spiral section. Two-point tread and flange contact occurs at the trailing outer wheel at t = 3.375 sec (i.e., 2 ft into the constant radius curve).

Figure 3b shows the angle of attack histories of the four wheelsets of the vehicle. As the vehicle enters the curve, the wheelsets of the front truck initially develop positive angles of attack. The wheelsets of the rear truck, which are still on tangent track, have zero angles. During negotiation of the transition spiral track, the angles of attack of all the wheelsets display oscillatory behavior. The oscillations decay as the vehicle negotiates the constant radius curve track. In steady-state conditions, the leading wheelsets of the front and rear trucks develop angles of attack of ~ 0.33 deg and the trailing wheelsets develop angles of ~ 0.06 deg.

The lateral force at the leading outer wheel of the vehicle as a function of time is shown in Figure 4a. The force increases rapidly at t = 1.375 sec when the leading outer wheel hits the flange and two-point contact develops. The force continues to increase, reaching a maximum of 5270 lb at t = 3.250 sec (i.e., 146 ft into the spiral) just before entering the constant radius curve. The peak force exceeds the steady-state force by 17%.

The leading outer wheel, front truck, and vehicle work as a function of time are shown in Figure 4b. The front truck work is the sum of the work expended at the contact patches at the four wheels of the front truck; similarly, the vehicle work is the sum of the work at all contact patches. At t = 1.375 sec, two-point contact develops at the leading

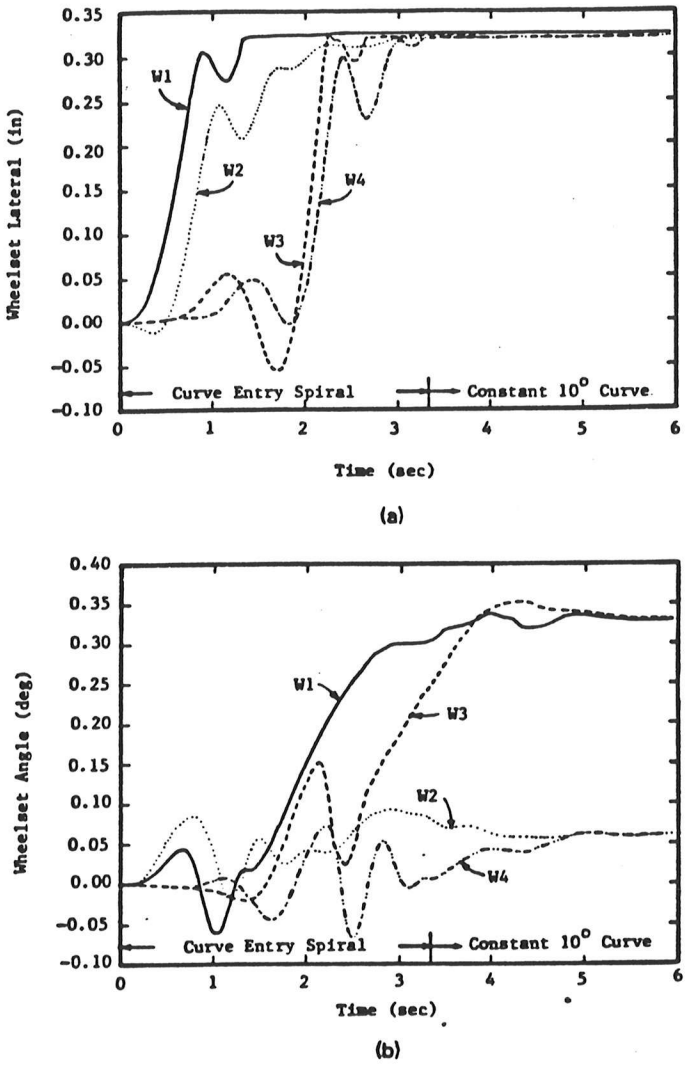

Figure 3. History of (a) Wheelset Lateral Excursions and (b) Angles of Attack of a Conventional Vehicle with New AAR Wheels Negotiating a 150 ft Curve Entry Spiral into a 10° Curve at a Balance Speed of 45 ft/sec.

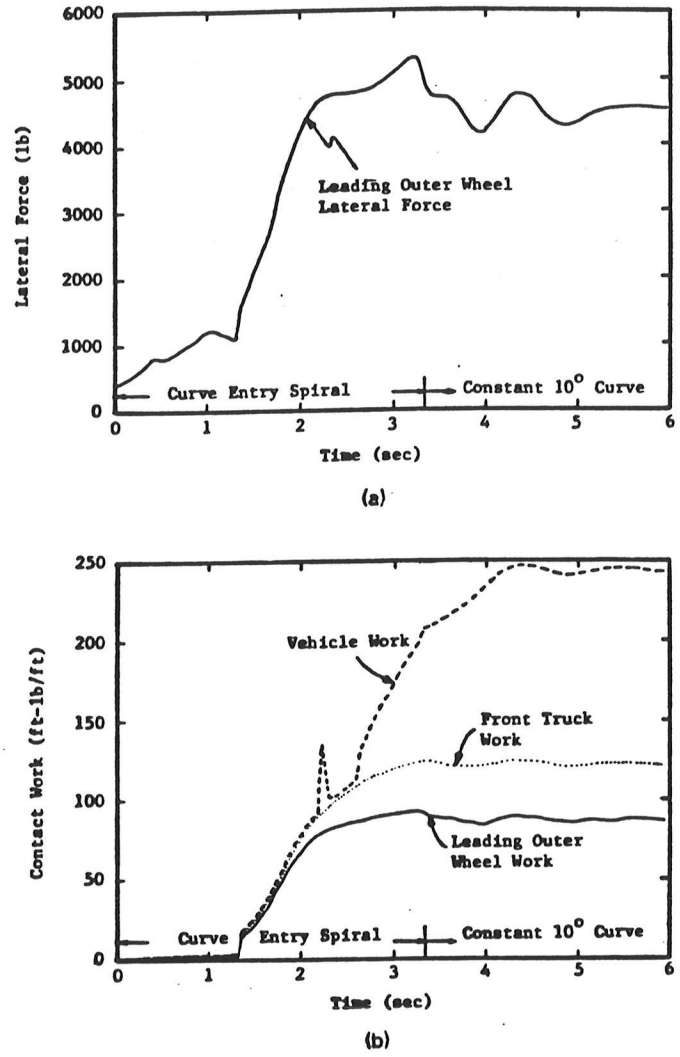

Figure 4. History of (a) Leading Outer Wheel Lateral Force and (b) Contact Work of a Conventional Vehicle with New AAR Wheels Negotiating a 150 ft Curve Entry Spiral into a 10° Curve at a Balance Speed of 45 ft/sec.

outer wheel, and the work function shows a sudden jump. As the vehicle continues through the curve, the contact work at the leading outer wheel and at the front truck continues to increase and each approaches a constant. The vehicle work rises rapidly at t = 2.250 sec when the leading outer wheel of the rear truck bounces into the flange and two-point contact occurs. The work decreases since single-point tread contact is restored and then increases at t = 2.750 sec when two-point contact again develops. The vehicle work continues to increase and then reaches a constant as steady-state conditions are approached.

A limited study of curve entry performance has been conducted to determine the effect of track curvature on the transient behavior. Table 2 summarizes the steady-state and peak flanging wheel force and contact work of a conventional vehicle with new AAR wheels entering 2.5° (2290 ft), 5° (1150 ft), and 10° (575 ft) curves at balance speed. As tighter curves are traversed, the dynamic effects diminish. The wheelsets displace to the outer rail and, upon reaching the flange clearance, remain there. In comparison, for negotiation of shallow curves, the wheelsets displace back and forth approaching the flanges but always remain in tread contact. The wheelsets exhibit "hunting"-type oscillations along the transition spiral, resulting in significant dynamic behavior.

A study of the effect of spiral length on the peak flanging wheel lateral force has been conducted. In the study, a conventional vehicle with new AAR wheels negotiates a transition spiral of varying length into a 10° curve at a balance speed of 45 ft/sec. The peak flanging force as a function of spiral length is shown in Figure 5. Reducing the spiral length increases the peak lateral force resulting from the initial flange contact. For short spiral lengths less than 75 ft, the peak force significantly exceeds the steady-state force. As the spiral length increases, the peak lateral force decreases and approaches the steady-state flange force.

Table 2. Performance of a Conventional Vehicle with New AAR Wheels Negotiating a 150 ft Curve Entry Spiral into a 2.5°, 5°, and 10° Curve at Balance Speed.

DEGREE CURVE (deg)	LEADING OUTER WHEEL LATERAL FORCE (lb)			LEADING OUTER WHEEL WORK (ft-lb/ft)		
	Steady-State	Peak	% Increase	Steady-State	Peak	% Increase
2.5°	340	1660	388%	1	2	100%
5°	2060	2650	29%	36	41	14%
10°	4520	5270	17%	87	93	7%

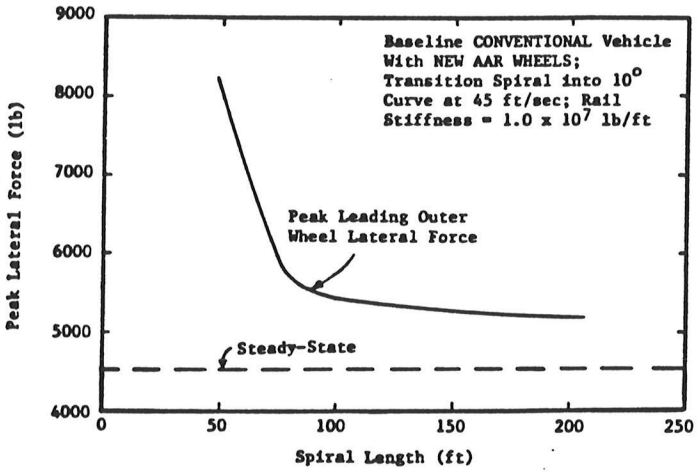

Figure 5. Effect of Curve Entry Spiral Length on the Peak Lateral Wheel Force of a Conventional Vehicle with New AAR Wheels Entering a 10° Curve at a Balance Speed of 45 ft/sec.

Performance of Forced-Steered Vehicle

A dynamic simulation has been conducted to determine the curve entry performance of a forced-steered vehicle with Heumann wheels negotiating a 150 ft spiral into a 10° curve at a balance speed of 45 ft/sec. Figures 6a and b show response histories of wheelset lateral excursions and angles of attack, respectively. Figures 7a and b show histories of flanging wheel force and contact work, respectively.

As the vehicle enters the curve, the leading and trailing wheelsets of the front truck displace toward the outer rail but maintain tread contact. The maximum lateral excursion occurs for the leading wheelset at t = 3.250 sec (i.e., 146 ft into the spiral curve) and is 0.248 in. The lateral displacements of the leading and trailing wheelsets of the rear truck increase and decrease slightly and then develop positive excursions. The steady-state excursions are ~ 0.158 in for the trailing wheelsets of the two trucks.

Figure 6b shows the wheelset angles of attack as a function of time. Very small angles of attack develop during the simulation. The largest magnitude is 0.073 deg, which occurs for the leading wheelset of the front truck at t = 2.875 sec (i.e., 129 ft into the spiral curve). In the curve entry spiral, the angles of attack of all wheelsets oscillate about near radial positions. In the constant radius curve, the leading wheelsets of the front and rear trucks develop positive angles of attack; the trailing wheelsets approach perfect radial alignment. The steady-state angles are ~ 0.002 deg for the trailing wheelsets of the two trucks. The forced-steering action successfully positions the trailing wheelsets radially (since minimal flange forces act on the trailing wheelsets).

The lateral force of the leading outer wheel is shown in Figure 7a. The force is characterized by significant oscillations. The force increases to a maximum of 1820 lb at t = 2.250 sec (i.e., 101 ft into the spiral curve). As the vehicle enters the constant radius curve, the force decreases and reaches a steady-state value of 1350 lb. The peak force exceeds the steady-state force by 35%.

The work at the leading outer wheel, the front truck, and the vehicle is shown in Figure 7b. In comparison to the work expended by the other vehicles in previous simulations, the work for the forced-steered vehicle with Heumann wheels is very small. The maximum values of work are 7, 13, and 22 ft-lb/ft for the leading outer wheel, front truck, and total vehicle, respectively. The work values in steady-state are 6, 7, and 14 ft-lb/ft, respectively.

Comparative Vehicle Performance

Curving performance data in terms of the steady-state and peak values of the leading outer wheel lateral force and contact work are summarized in Tables 3 and 4 for vehicles with new AAR and Heumann wheels, respectively. The tables show that the forced-steered vehicle offers improved performance in terms of decreased steady-state and peak forces and work in comparison to the conventional and self-steered vehicles. For example, the peak work level is 55 ft-lb/ft for the forced-steered vehicle compared to 93 and 75 ft-lb/ft for the conventional and self-steered vehicles, respectively, (for vehicles with new AAR wheels negotiating a 150 ft spiral into a 10° curve at a balance speed of 45

Table 3. Dynamic Curve Entry Performance of Conventional, Self-Steered, and Forced-Steered Vehicles with New AAR Wheels Negotiating a 150 ft Spiral into a 10° Curve at a Balance Speed of 45 ft/sec.

NEW AAR WHEELS

	CONVENTIONAL			SELF-STEERED RADIAL			FORCED-STEERED RADIAL		
	Steady-State	Peak	% Increase	Steady-State	Peak	% Increase	Steady-State	Peak	% Increase
Flanging Wheel Lateral Force (lb)	4520	5270	17	4260	5090	20	3480	4310	24
Flanging Wheel Work (ft-lb/ft)	87	93	7	67	75	12	48	55	15

Table 4. Dynamic Curve Entry Performance of Conventional, Self-Steered, and Forced-Steered Vehicles with Heumann Wheels Negotiating a 150 ft Spiral into a 10° Curve at a Balance Speed at 45 ft/sec.

HEUMANN WHEELS

	CONVENTIONAL			SELF-STEERED RADIAL			FORCED-STEERED RADIAL		
	Steady-State	Peak	% Increase	Steady-State	Peak	% Increase	Steady-State	Peak	% Increase
Flanging Wheel Lateral Force (lb)	4050	4950	22	3940	4800	22	1350	1820	35
Flanging Wheel Work (ft-lb/ft)	62	72	16	56	64	14	6	7	17

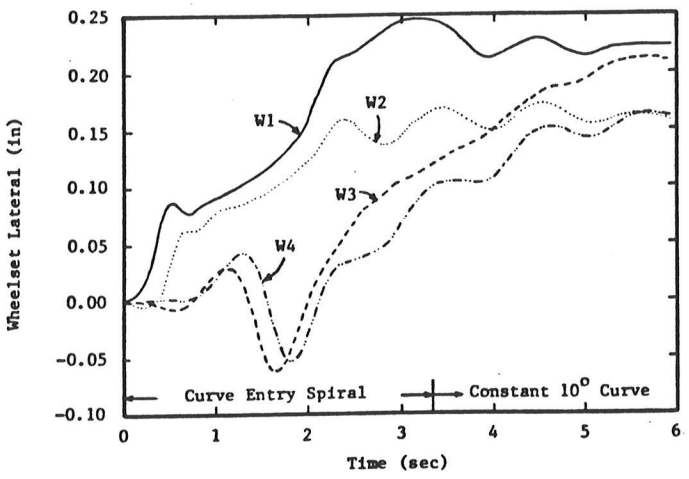

(a)

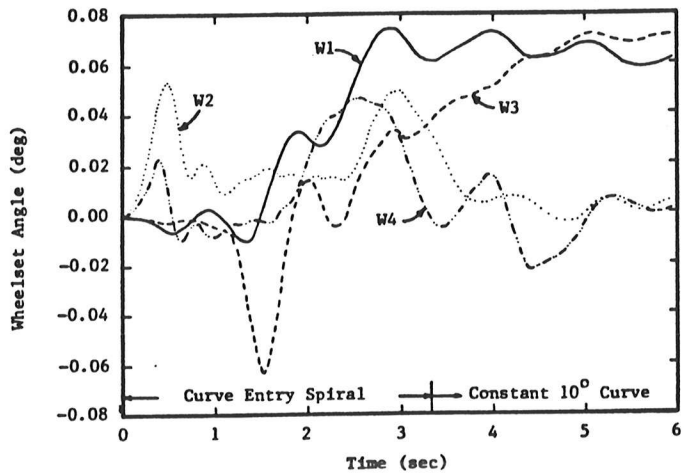

(b)

Figure 6. History of (a) Wheelset Lateral Excursions and (b) Angles of Attack of a Forced-Steered Vehicle with Heumann Wheels Negotiating a 150 ft Curve Entry Spiral into a 10° Curve at a Balance Speed of 45 ft/sec.

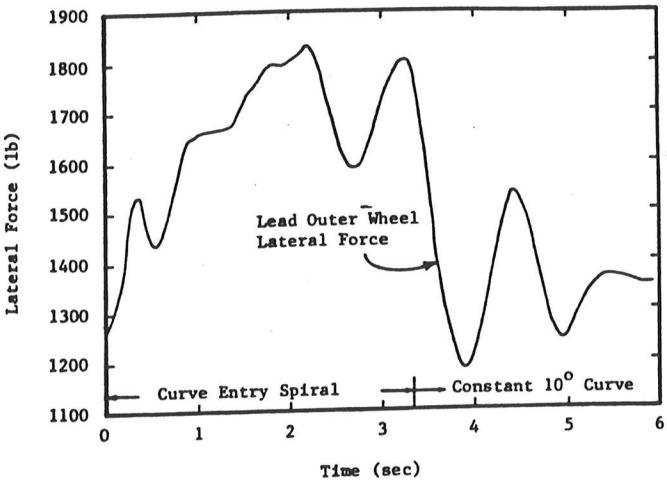

(a)

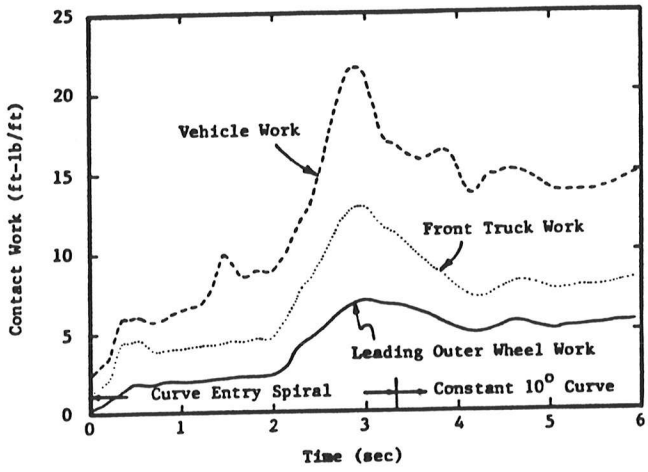

(b)

Figure 7. History of (a) Leading Outer Wheel Lateral Force and (b) Contact Work of a Forced-Steered Vehicle with Heumann Wheels Negotiating a 150 ft Curve Entry Spiral into a 10° Curve at a Balance Speed of 45 ft/sec.

ft/sec). The tables also show that the peak/steady-state force and work ratios are highest for the forced-steered vehicle (in terms of percent increase). For example, for vehicles with new wheels, the peak work exceeds the steady-state work by 15% for the forced-steered vehicle and by 7 and 12% for the conventional and self-steered vehicles, respectively. Table 4 shows that the greatest improvement in performance is obtained with the forced-steered vehicle with Heumann wheels. The steady-state and peak values of work are 6 and 7 ft-lb/ft, respectively. However, this vehicle experiences the largest dynamic overshoot in terms of percent. The peak work exceeds the steady-state work by 17%, and the peak lateral force exceeds the steady-state force by 35%.

The results of Tables 3 and 4 suggest that significant performance improvements can be achieved by employing forced-steered vehicles with Heumann type wheels. Forced-steered vehicles experience a higher ratio of dynamic to steady-state force in curve entry than conventional and self-steered vehicles. However, the magnitudes of the transient responses of the forced-steered vehicles are smaller than those that develop for the conventional and self-steered vehicles, suggesting that the increased dynamic behavior can be accepted.

CONCLUSIONS

The results of this paper show that although transient characteristics occur, the predictions of steady-state analyses are essentially substantiated. First, vehicles with steered trucks, particularly forced-steered trucks, reduce wheelset angles, wheel/rail contact force and work implying improved performance compared to conventional vehicle performance. Second, wheel profiles which maintain single-point contact, such as the Heumann wheel profile, reduce work expended during curve negotiation and are potentially advantageous compared to two-point contact profiles.

ACKNOWLEDGEMENTS

Support for the work described in this paper was provided by the U. S. Department of Transportation (DOT) Transportation Systems Center (TSC) and by the Urban Mass Transportation Administration (UMTA).

REFERENCES

1. Boyd, P.L., Zaiko, J.P., and Jordan, W.L., "Effect of Wheel Taper and Primary Suspension Stiffness on Wheel/Rail Forces at the Washington Metropolitan Area Transit Authority," Vol. II, Test Report, U.S.D.O.T. Interim Report, March, 1980.
2. Mekosh, G., "Design Feasibility Study for Modifying an Existing Heavy Rapid Rail Truck to a Steerable Configuration," Budd Company Project Memorandum, Report No. DOT-TSC-UM104-PM-80-49, December 1980.
3. Elkins, J.A., and Allen, R.A., "Testing a Transit Vehicle for Wheel and Rail Wear,"ASME Paper 81-WA/DSC-19, 1981.
4. Elkins, J.A., and Eickhoff, B.M., "Advances in Non-Linear Wheel/Rail Force Prediction Methods and Their Validation," Journal of Dynamic Systems, Measurement, and Control, Vol. 104, No. 2, June 1982, pp. 133-142.
5. Scheffel, H., "Self-Steering Wheelsets Will Reduce Wear and Permit Higher Speeds," Railway Gazette International, December 1976, pp. 453-456.
6. Doyle, G.R., "Conventional Versus Self-Steering Radial Truck for High-Speed Passenger Trains," ASME Paper 79-RT-3, 1979.
7. Horak, D., Bell, C.E., and Hedrick, J.K., "A Comparison of the Stability and Curving Performance of Radial and Conventional Rail Vehicle Trucks," Journal of Dynamic Systems, Measurement, and Control, Vol. 103, September 1981, pp. 191-200.
8. Smith, R.E., and Anderson, R.J., "Properties of Cross-Braced Trucks," ASME Paper 82-WA/DSC-21, 1982.
9. Scales, B.T., "Behavior of Bogies on Curves," Railway Engineering Journal, Vol. 1, July 1972, pp. 19-24.
10. List, H.A., "Means for Improving the Steering Behavior of Railway Vehicles," presented to the Annual Meeting of the Transportation Research Board, January 22, 1976.
11. Bell, C.E., and Hedrick, J.K., "Forced-Steering of Rail Vehicles: Stability and Curving Mechanics," Vehicle System Dynamics, Vol. 10, 1981, pp. 357-386.
12. Illingworth, R., and Pollard, M.G., "The Use of Steering Axle Suspensions to Reduce Wheel and Rail Wear in Curves," Proc. Inst. Mech. Eng., Vol. 196, 1982, pp. 379-385.
13. Marcotte, P.P., Mathewson, K.J., and Caldwell, W.N., "Improved Wheel Tread Profiles for Heavy Freight Vehicles," J. of Engineering for Industry, Vol. 102, August 1980, pp. 263-271.
14. Cooperrider, N.K., and Wirth, J.L., "Wheel Tread Profile as a Rail Vehicle Design Parameter," ASME Paper 82-WA/DSC-3, 1982.
15. Elkins, J.A., and Weinstock, H., "The Effects of Two-Point Contact on the Curving Behavior of Railroad Vehicles," presented at the 1982 ASME Winter Annual Meeting, Phoenix, Arizona, November 1982.
16. Nagurka, M.L., Bell, C.E., Hedrick, J.K., and Wormley, D.N., "Computational Methods for Rail Vehicle Steady-State Curving Analysis," Computational Methods in Ground Transportation Vehicles, ed. Kamal, M., and Wolf, J., ASME AMD-Vol. 50, 1982, pp. 153-179.
17. Wormley, D.N., Hedrick, J.K., and Nagurka, M.L., "Stability and Curving Performance of Conventional and Advanced Rail Transit Vehicles," U.S. DOT Report, DTRS 57-80C-00152, November 1982.
18. Nagurka, M.L., Hedrick, J.K., and Wormley, D.N., "Curving Performance of Rail Transit Trucks," Proceedings of the Eighth IAVSD-IUTAM Symposium on the Dynamics of Vehicles on Roads and Tracks, Cambridge, MA, August 15-19, 1983, pp. 377-389.
19. Smith, K., "Curve Entry and Curve Negotiation Characteristics of Two-Axle Trucks," M.S. Thesis, Illinois Institute of Technology, December 1975.
20. Law, E.H., and Cooperrider, N.K., "Nonlinear Dynamic and Steady-State Curving of Rail Vehicles," presented at the 1980 ASME Winter Annual Meeting, San Francisco, CA, December 1978.
21. Cooperrider, N.K., and Law, E.H., "The Nonlinear Dynamics of Rail Vehicles in Curve Entry and Negotiation," presented at the Seventh IAVSD-IUTAM Symposium on the Dynamics of Vehicles on Roads and Tracks, Cambridge, U.K., September 7-11, 1981.
22. Clark, R.A., Eickhoff, B.M., and Hunt, G.A., "Prediction of the Dynamic Response of Vehicles to Lateral Track Irregularities," presented at the Seventh IAVSD-IUTAM Symposium on the Dynamics of Vehicles on Roads and Tracks, Cambridge, U.K., September 7-11, 1981.
23. Duffek, W., and Jaschinski, A., "Efficient Implementation of Wheel-Rail Contact Mechanics in Dynamic Curving," presented at the Seventh IAVSD-IUTAM Symposium on the Dynamics of Vehicles on Roads and Tracks, Cambridge, U.K., September 7-11, 1981.
24. Fortin, J.A.C., and Anderson, R.J., "Steady-State and Dynamic Predictions of the Curving Performance of Forced-Steering Rail Vehicles," Proceedings of the Eighth IAVSD-IUTAM Symposium on the Dynamics of Vehicles on Roads and Tracks, Cambridge, MA, August 15-19, 1983, pp. 179-192.
25. Ahlbeck, D.R., "The Effects of Track Modulus on Vehicle-Track Dynamic Interaction," IEEE/ASME Joint Railroad Conference, Erie, PA, April 1982.
26. Nagurka, M.L., "Curving Performance of Rail Passenger Vehicles," Ph.D. Thesis, Dept. of Mechanical Engineering, M.I.T., Cambridge, MA, May 1983.
27. Cooperrider, N.K., and Law, E.H., "Data Book: Wheel/Rail Geometry for Five Wheel Profiles and Three Rail Profiles," Report No. ERC-R-75015, Dept. of Mechanical Engineering, Arizona State University, Tempe, AZ.